Politecnico di Milano
AUTOMATION AND CONTROL ENGINEERING

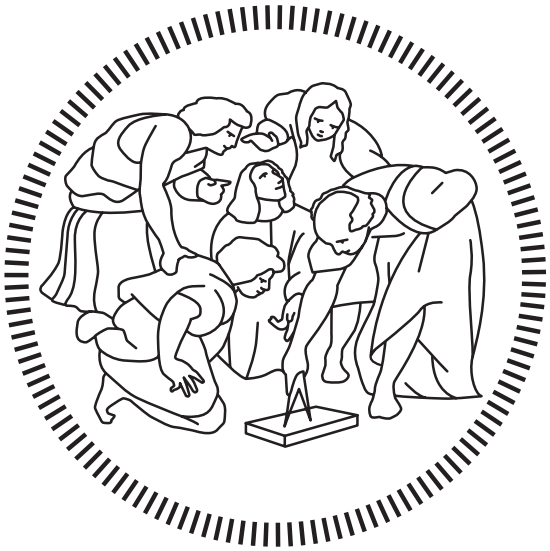

Study and Control of the Mechanichal System: Rotary Flexible Joint

Course
Automation and Control Laboratory

Student
Andrea Archetti – 10616682
Alp Recep Dayan – 10823110
Alessandro Firetto – 10633148
Jesucristo Torres Toledo – 10822036

Academic Year 2022 – 2023

Contents

Problem Description

This report will describe the model of the system, our solution and some attempts to describe and control the system.

The system is composed of a DC motor that provides torque to a metal base, over which a metal arm is fixed with an hinge and two symmetrical springs.

The length of the arm, hence its inertia, and the the equilibrium length of the springs can be modified in a variety of different configurations.

The system has several interfaces that could be connected to an acquisition system (DAC/ADC + Amplifier) to acquire measurements and provide input signal, namely:

- Actuators:

  Voltage driven DC motor;

- Sensors:

  Incremental Encoder for the position of the base with respect to the global reference frame;

  Incremental Encoder for the relative position of the arm with respect to the base.

The acquisition system composed by ADC/DAC + Amplifier model is out of the scope of this report.

In the tables below we can see respectively the datasheet for the motor and for the flexible joint:

Symbol	Description	Value	Variation
V_{nom}	Motor nominal input voltage	6.0 V	
R_m	Motor armature resistance	2.6 Ω	± 12%
L_m	Motor armature inductance	0.18 mH	
k_t	Motor current-torque constant	7.68×10^{-3} N-m/A	± 12%
k_m	Motor back-emf constant	7.68×10^{-3} V/(rad/s)	± 12%
K_g	High-gear total gear ratio	70	
	Low-gear total gear ratio	14	
η_m	Motor efficiency	0.69	± 5%
η_g	Gearbox efficiency	0.90	± 10%
$J_{m,rotor}$	Rotor moment of inertia	3.90×10^{-7} kg-m^2	± 10%
J_{tach}	Tachometer moment of inertia	7.06×10^{-8} kg-m^2	± 10%
J_{eq}	High-gear equivalent moment of inertia without external load	2.087×10^{-3} kg-m^2	
	Low-gear equivalent moment of inertia without external load	9.7585×10^{-5} kg-m^2	
B_{eq}	High-gear Equivalent viscous damping coefficient	0.015 N-m/(rad/s)	
	Low-Gear Equivalent viscous damping coefficient	1.50×10^{-4} N-m/(rad/s)	
m_b	Mass of bar load	0.038 kg	
L_b	Length of bar load	0.1525 m	
m_d	Mass of disc load	0.04 kg	
r_d	Radius of disc load	0.05 m	
m_{max}	Maximum load mass	5 kg	
f_{max}	Maximum input voltage frequency	50 Hz	
I_{max}	Maximum input current	1 A	
ω_{max}	Maximum motor speed	628.3 rad/s	

Symbol	Description	Value	Unit
	Module Dimensions	10 x 8 x 5	cm^3
L_1	Main arm length	29.8	cm
L_2	Load arm length	15.6	cm
	Distance between joint to middle of load arm		
d_{12}	Arm Anchor Point 1	21.0	cm
d_{12}	Arm Anchor Point 2	23.5	cm
d_{12}	Arm Anchor Point 3	26.0	cm
	Module body mass	0.3	kg
m_1	Main arm mass	0.064	kg
m_2	Load arm mass	0.03	kg
K_{enc}	Encoder resolution (in quadrature mode)	4096	Counts/Rev
K_1	Spring #1 stiffness	187	N/m
K_2	Spring #2 stiffness	313	N/m
K_3	Spring #3 stiffness	565	N/m

The main task of this project is to provide a basic control strategy for such system and to develop a more advanced control strategy to accommodate all possible configurations of the system in question.

This goal is divided in sub-tasks to be achieved:

1. position control of the base, with a frequency based approach;
2. position control of the arm tip, with a frequency based or a state space approach;
3. manage uncertainties and control the position of the arm tip with the system in different configurations, with a state space approach or other advanced control techniques.

Model Identification

The system could be schematized as:

It is possible to recognize models of a DC motor powered by a voltage V_{dc} coupled with a gearbox (both modeled in the same box) that provides torque u to the flexible joint. Finally two encoders read the angular positions y and send the estimated values $\hat{y}$ to the ADC converter.

2.1 Mathematical Model

2.1.1 DC motor equations

Before starting to model the DC motor we can get the time constant of its dynamics from the values in the datasheet:

$$\frac{R}{L} = \frac{2.6\,\Omega}{0.18\,mH} \approx 15\,KHz$$

As this is clearly above the frequency range of the mechanical system, we can neglect its dynamics and model only the static contribution.

The physical equations of the DC Motor then become:

$$\begin{cases} V_a = R_a I_a + E \\ E = k_m \dot{\theta} \\ \tau = k_t I_a \end{cases}$$

After several mathematical steps and considering the gearbox ratio K_g and the conversion efficiencies we get:

$$\tau = \frac{\eta_m \eta_g k_t K_g (V - K_g k_m \dot{\theta})}{R_m}$$

Where τ is the torque applied to the system and θ is the angular position of the base.

2.1.2 Flexible joint equations

We can represent our system as follows:

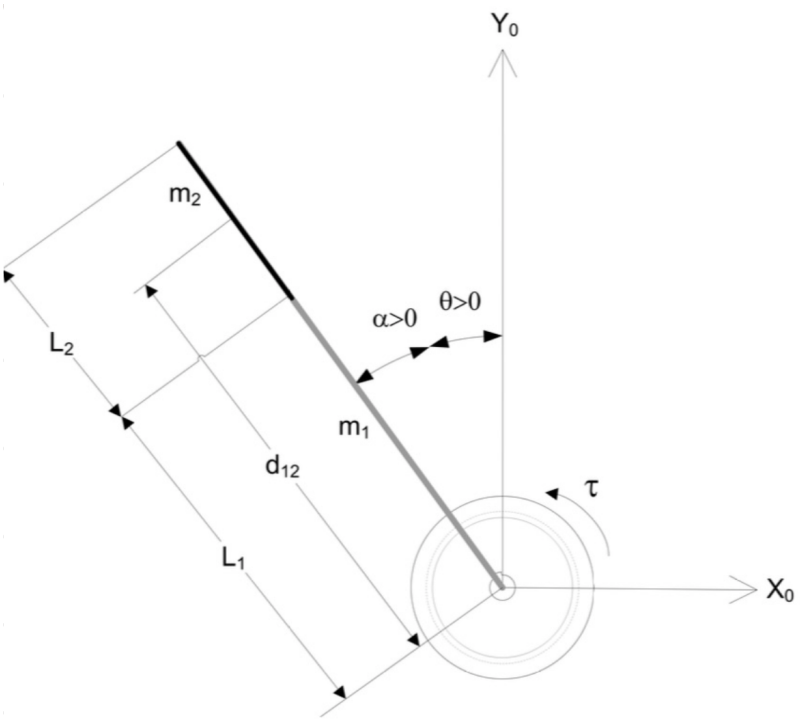

Here we have a 2-dofs mechanical system that can be modelled using a Lagrangian approach.

The 2 deegrees of freedom are:

- θ: the absolute angular position of the base;
- α: the relative angular position of the arm with respect to to the base.

The kinetic energy:

$$T = \frac{1}{2} J_{eq} \dot{\theta}^2 + \frac{1}{2} J_L (\dot{\theta} + \dot{\alpha})^2$$

where J_{eq} refers to the equivalent inertia of the motor + gearbox, and J_L refers to the inertia of the arm.

The Potential Energy:

$$V = \frac{1}{2} K_s \dot{\alpha}^2$$

where K_s refers to the linearized stiffness of the equivalent torsional spring.

The Dissipative Function:

$$D = \frac{1}{2} B_{eq} \dot{\theta}^2 + \frac{1}{2} B_L \dot{\alpha}^2$$

where B_{eq} and B_L refer respectively to the equivalent friction of the motor + gearbox and the equivalent friction of the arm.

The dynamics of the system can be found applying the Euler-Lagrange equations for each deegree of freedom :

$$\frac{d}{dt}\left(\frac{\partial T}{\partial \dot{x}}\right) - \left(\frac{\partial T}{\partial x}\right) + \left(\frac{\partial D}{\partial \dot{x}}\right) + \left(\frac{\partial V}{\partial x}\right) = \left(\frac{\delta W}{\delta x}\right)$$

finally we get the following system of equation:

$$\begin{cases} J_{eq}\ddot{\theta} + J_L(\ddot{\theta} + \ddot{\alpha}) + B_{eq}\dot{\theta} = \tau \\ J_L(\ddot{\theta} + \ddot{\alpha}) + B_L\dot{\alpha} + K_s\alpha = 0 \end{cases}$$

Non-Linear model of the springs

Until now we have modeled the two linear springs as an equivalent torsional one in order to reduce the complexity of the system.

To prove the validity of this assumption we can consider Hooke's law:

$$F = -K_s(x_k - x_0)$$

Thanks to the symmetry of the system, studying the behaviour of a single spring is enough to model both of them.

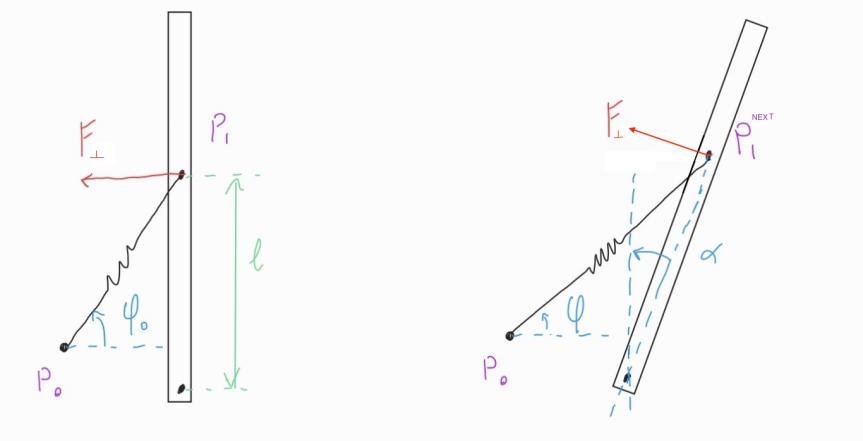

In the left figure the equilibrium position is $x_k = x_0$, where:

$$\varphi_0 = atan\left(\frac{P_{1_y}}{P_{0_x}}\right)$$

$$F_\perp = F \cdot cos(\varphi_0)$$

$$x_0 = \sqrt{(P_{1_x} - P_{0_x})^2 + (P_{1_y} - P_{0_y})^2}$$

In the right the system is in a perturbed position, so:

$$x_k = \sqrt{(P_{1_x} - P_{0_x})^2 + (P_{1_y} - P_{0_y})^2} \rightarrow \Delta x_k = x_k - x_0$$

$$P_1^{NEXT} = \begin{bmatrix} l \cdot sin(\alpha) \\ l \cdot (1 - cos(\alpha)) \end{bmatrix} \rightarrow F_\perp = F \cdot cos(\varphi + \alpha)$$

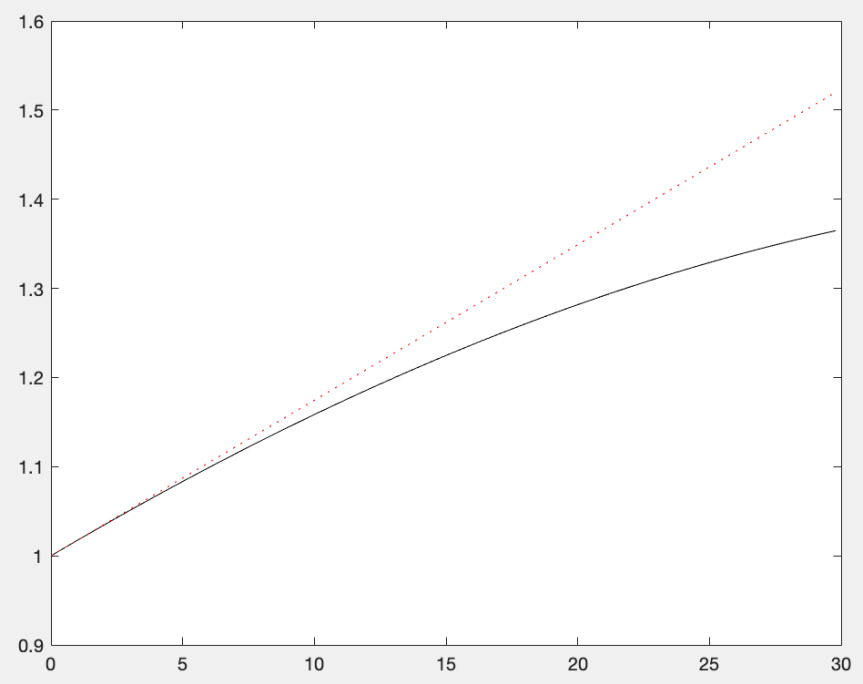

The plot above represents the value of the $F_\perp$ as function of the angle α and its linear approximation at the origin.

The error between the two curves is expressed by the curve below:

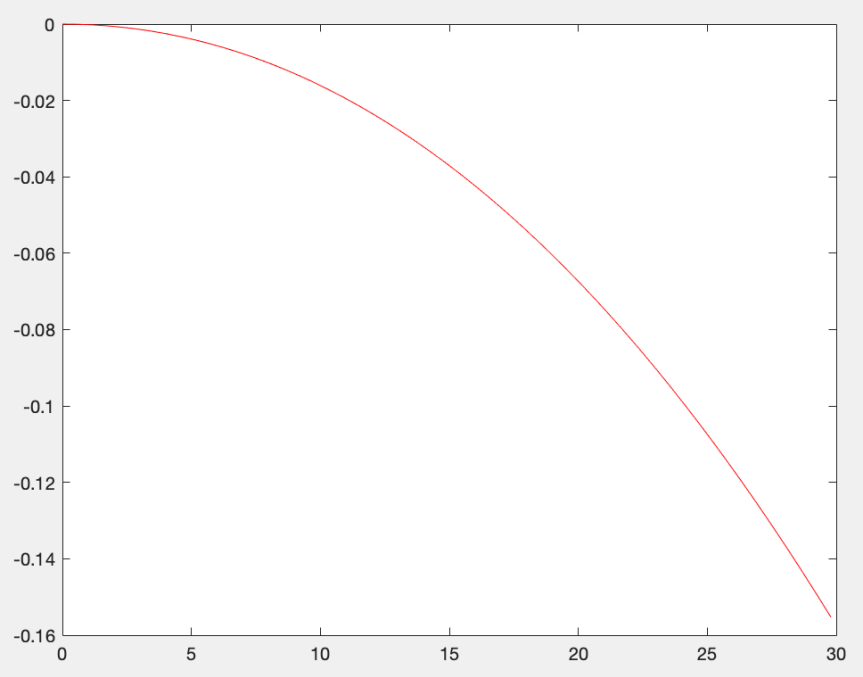

As we can see, while α is below 25° the error between the two models is less than 10%. As the tip's angle always remained below 10° in our measurements, the linear model introduced before is precise enough to represent our system.

2.1.3 State Space Representation

Continuous time

Starting from the aforementioned equations:

$$\begin{cases} J_{eq}\ddot{\theta} + J_L(\ddot{\theta} + \ddot{\alpha}) + B_{eq}\dot{\theta} = \frac{\eta_m \eta_g k_t K_g (V - K_g k_m \dot{\theta})}{R_m} \\ J_L(\ddot{\theta} + \ddot{\alpha}) + B_L\dot{\alpha} + K_S\alpha = 0 \end{cases}$$

we develop the State Space system in continuous time, having as states the following array:

$$\begin{bmatrix} \theta \\ \dot{\theta} \\ \alpha \\ \dot{\alpha} \end{bmatrix}$$

the A matrix:

$$\begin{bmatrix} 0 & 1 & 0 & 0 \\ 0 & -\frac{\eta_m \eta_g k_t k_m K_g^2 + B_{\text{eq}} R_m}{J_{\text{eq}} R_m} & \frac{K_s}{J_{\text{eq}}} & \frac{B_L}{J_{\text{eq}}} \\ 0 & 0 & 0 & 1 \\ 0 & \frac{\eta_m \eta_g k_t k_m K_g^2 + B_{\text{eq}} R_m}{J_{\text{eq}} R_m} & -K_S\left(\frac{J_{\text{eq}} + J_L}{J_{\text{eq}} J_L}\right) & -B_L\left(\frac{J_{\text{eq}} + J_L}{J_{\text{eq}} J_L}\right) \end{bmatrix}$$

and the B matrix:

$$\begin{bmatrix} 0 \\ \frac{\eta_m \eta_g k_t K_g}{R_m J_{\text{eq}}} \\ 0 \\ -\frac{\eta_m \eta_g k_t K_g}{R_m J_{\text{eq}}} \end{bmatrix}$$

Considering as the outputs of the system the angular positions θ and α.

Discrete time

In order to apply optimization techniques on our data in order to find the parameters of the system, we need a state space representation in discrete time. To do so we apply the forward Euler method considering a sampling time Δ.

Our discrete time A matrix becomes then:

$$\begin{bmatrix} 1 & \Delta & 0 & 0 \\ 0 & 1 - \Delta\frac{\eta_m \eta_g k_t k_m K_g^2 + B_{eq} R_m}{J_{eq} R_m} & \Delta\frac{K_s}{J_{eq}} & \Delta\frac{B_L}{J_{eq}} \\ 0 & 0 & 1 & \Delta \\ 0 & \Delta\frac{\eta_m \eta_g k_t k_m K_g^2 + B_{\text{eq}} R_m}{J_{\text{eq}} R_m} & -\Delta K_S\left(\frac{J_{\text{eq}} + J_L}{J_{\text{eq}} J_L}\right) & 1 - \Delta B_L\left(\frac{J_{\text{eq}} + J_L}{J_{\text{eq}} J_L}\right) \end{bmatrix} \tag{2.1}$$

whereas the B matrix becomes:

$$\begin{bmatrix} 0 \\ \Delta\frac{\eta_m \eta_g k_t K_g}{R_m J_{\text{eq}}} \\ 0 \\ -\Delta\frac{\eta_m \eta_g k_t K_g}{R_m J_{\text{eq}}} \end{bmatrix}$$

while the outputs are still θ and α.

2.2 Identification Techniques

2.2.1 The CVX package

To infer the parameters of the state space representation from the data we used an optimization approach based on the CVX Matlab package, which allows us to optimize a convex cost function subjected to constraints in the form:

$$\begin{aligned} &\text{minimize} \left\| Ax - b \right\|_2 \\ &\text{subject to} \, Cx = d \\ &\left\| x \right\|_\infty \leq e \end{aligned}$$

2.2.2 Training Dataset

We used two different datasets to train our model, one for the identification at lower frequencies, one for higher ones.

2.2.3 The obtained model

2.2.4 Validation

2.2.5 Parameters estimation

Knowing that the shape of the matrix is the one expressed in 2.1 and knowing that the natural frequency and the damping coefficient of the system are respectively:

$$\begin{cases} \omega_n^2 = \frac{K_s}{J_{eq}} \\ 2\zeta\omega_n = \frac{B_L}{J_{eq}} \end{cases}$$

Which gives us:

$$\begin{cases} \omega_n = 24.1 \frac{rad}{s} \\ \zeta = 0.0176 \end{cases}$$

To validate our results we probed the system with a chirped sinusoidal signal with frequency varying from 1Hz to 10Hz and we extracted the Fourier transform of the tip position.

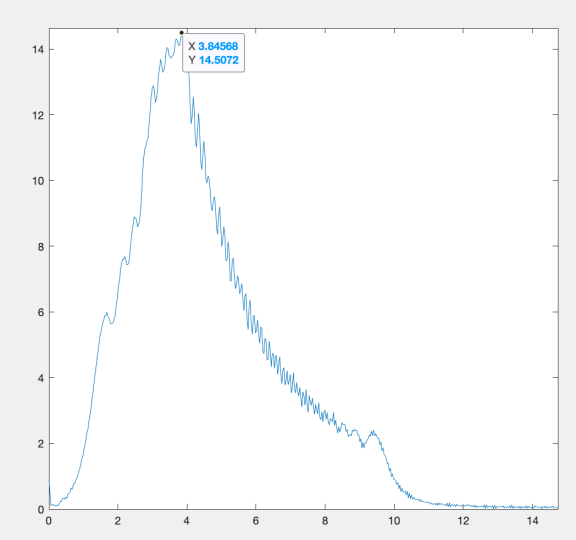

In the plot above we can see that we have a peak in the amplitude at the resonance frequency $f_n = 3.846\,Hz$ which gives us $\omega_n = 14.2\frac{rad}{s}$, almost the same we got with the optimization. This means that our model is able to describe the resonance of the actual system.

For the parameters of the rotating arm we compute the values of the inertia, following its geometry, as:

$$J_L = m_1 \cdot \frac{L_1^2}{3} + m_2 \cdot \frac{L_2}{12} + m_2 \cdot d^2 = 0.0032 Kgm^2$$

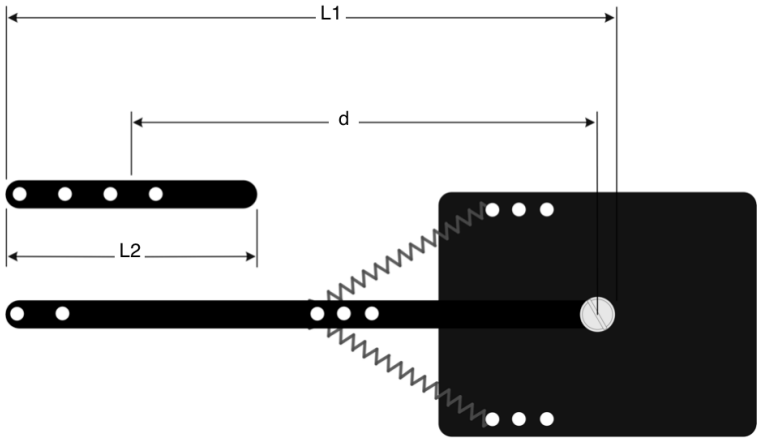

the value of the friction coefficient was supposed initially null:

$$B_L = 0$$

and the value of the K_s we use the value generated in the analysis stiffness identification:

the analysis provide a Fourier transfer of the second output (the relative position of the tip) as in the figure:

the peak is at:

$$f = 3.84568Hz$$

as result we assign the stiffness initial value as:

$$K_s = J_L \cdot \omega_n^2 = 1.8426N/m$$

Position Control of the Base

Our main objective regarding the control of the base is to achieve a set point tracking as fast as physically possible, while maintaining a phase margin $\phi_m \approx 60°$ to ensure robustness.

3.1 Controller Design

To do so we designed a controller based on the Bode diagram of the model of the system in open loop, represented in the image below:

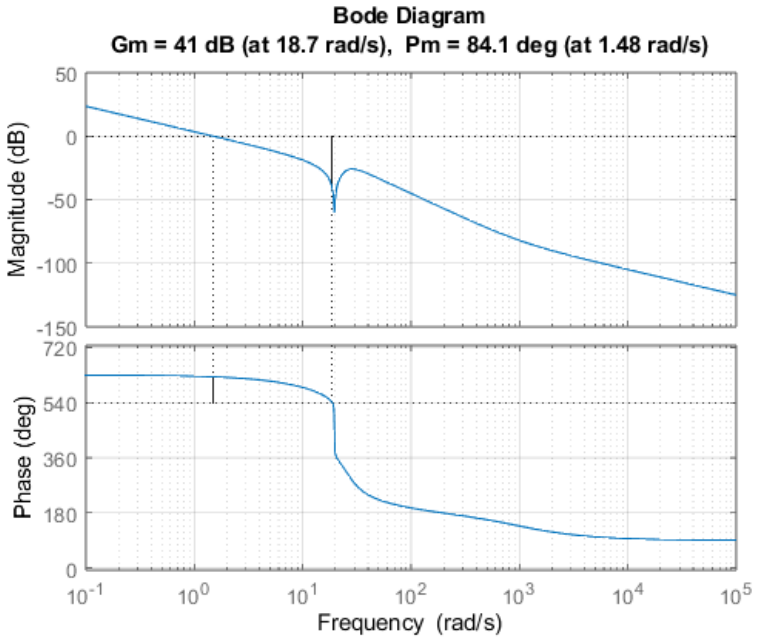

By looking at the pole-zero map below we can see that the dominant poles are the complex conjugate ones, which must be cancelled in order to speed up the response of the system.

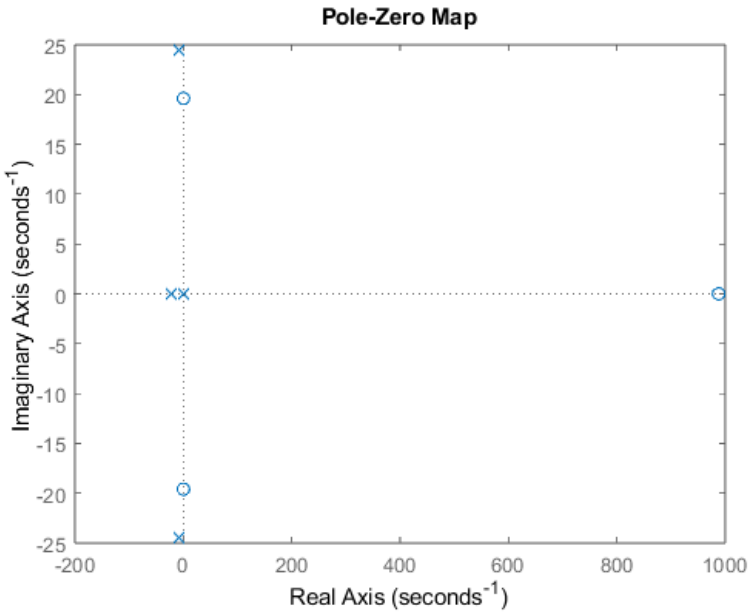

Even though the model itself presents a pole in the origin, an integral action in the controller is still needed in order to grant a zero steady state error, but doing so we drastically reduce the phase and make the system unstable. To fix this issue we added two poles right before the anti resonance in order to get the desired phase margin and, for feasibility reasons, two poles right after the resonance which also have the function to lower the peak at $\approx 30\frac{rad}{s}$.

Finally the overall gain of the controller is tweaked such that the crossing frequency is right before the anti-resonance, to get as much bandwidth as possible.

The controller transfer function is thus:

$$C = 150\frac{(s+7.43-24.5i)(s+7.43+24.5i)(s+3)^2}{s(s+22)^2(s+150)} \tag{3.1}$$

And the Bode diagram of the controlled system in open loop and its pole-zero map are respectively:

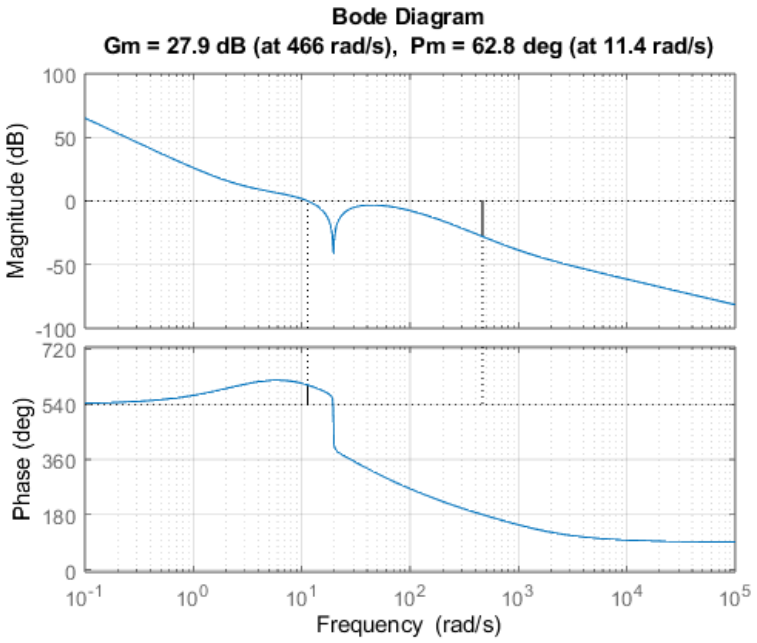

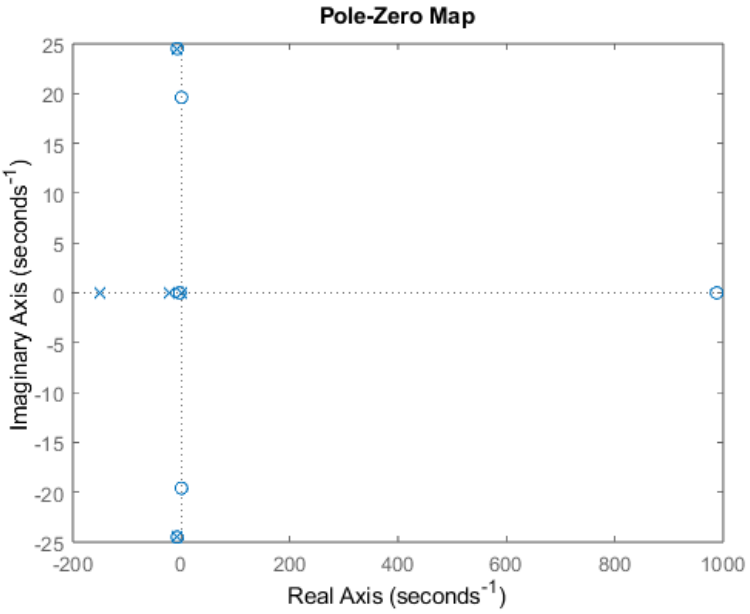

The overall control scheme is then:

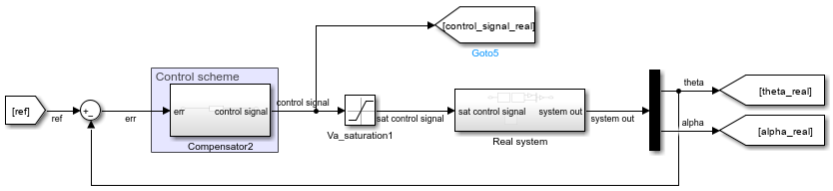

3.2 Validation

Now that we have developed a control scheme we have to verify that the closed loop system behaves accordingly to the specification imposed.

3.2.1 Step response

3.2.2 Frequency validation

By testing the system with sinusoidal references at fixed amplitudes and different frequencies we were able to reconstruct a Bode diagram for the actual closed loop system. The comparison between the experimental one and the theoretical one can be seen in the plot below:

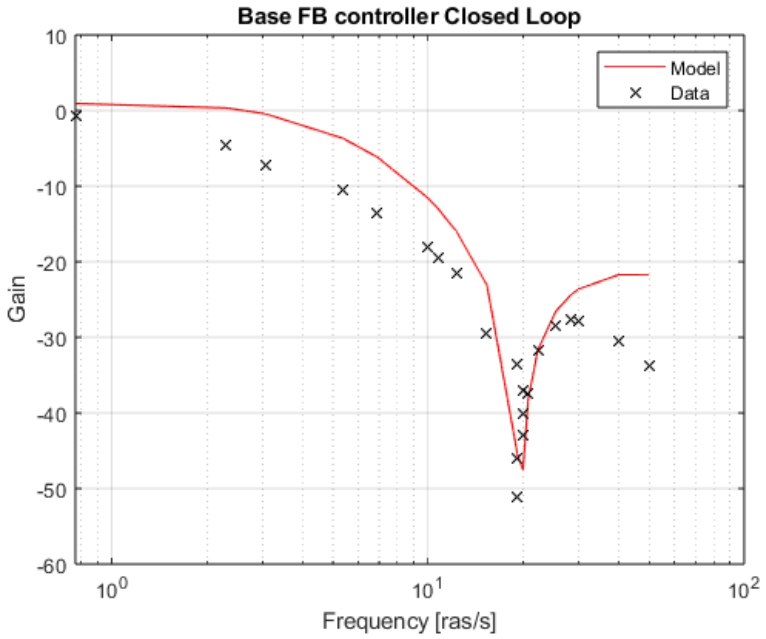

As we can see, at low frequencies the system is able to track the reference with small amplitude reduction up until $\approx 10 \frac{rad}{s}$ after which the signal is rejected.

Position Control of the Tip

In order to control the position of the tip we tried two different approaches: a frequency based one, like we did for the control of the position of the base, and a full state feedback control scheme.

4.1 Frequency Based Approach

Our goal is once again to track a set point for the position of the tip granting a phase margin $\approx 60°$ for robustness. This time we have a trade-off between speed of the controlled system and overshoot of the α angle and we decided to focus more on the latter option.

4.1.1 Controller Design

4.1.2 Step Response

4.1.3 Frequency Validation

4.2 State Estimators

In order to apply a full state feedback control scheme we must be able to know or to estimate the state of our system knowing only its outputs and inputs.

4.2.1 State Extractor

As our output is the array $\begin{bmatrix}\theta \\ \alpha\end{bmatrix}$ and the full state is $\begin{bmatrix}\theta \\ \dot{\theta} \\ \alpha \\ \dot{\alpha}\end{bmatrix}$, we could just apply a derivative to the output to get the full state, as expressed in the simulink scheme below.

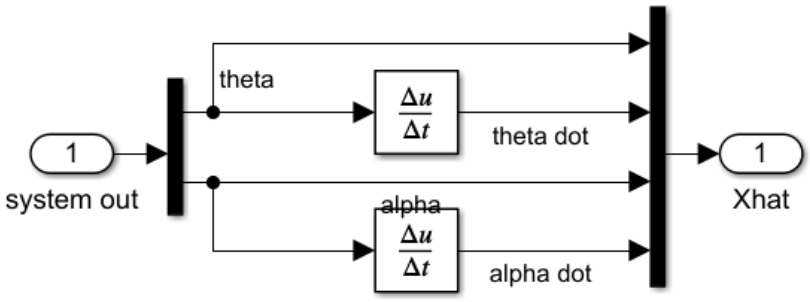

The benefits of such observer is that the estimation of the state is instantaneous and there is no dynamics for the error between the real and the estimated state.

The main drawback is that the derivative is done numerically, so high frequency noises in the measurements could lead to wrong state estimations. Luckily the sensors where precise enough so that the noise was not an issue, otherwise we would have introduced a low pass filter to mitigate it.

4.2.2 Luenberger Observer

In order to provide an estimation for the states of the

4.2.3 Kalman Filter

4.3 Pole Placement

4.3.1 Controller Design

4.3.2 Observers Comparison

4.3.3 Validation

Step Response

Frequency Validation

4.4 Linear Quadratic Regulator

The LQ regulator is an optimal full state feedback control scheme which has as control law:

$$u = -K_{LQR}x$$

Where K_{LQR} is found by solving this minimization problem:

$$\min_{u(\cdot)} \int_0^{t_1} \left(x^T Q x + u^T R u\right) dt$$

subject to $\dot{x} = Ax + Bu$

Where Q and R are matrices which represent respectively the weight on the state and on the inputs.

4.4.1 Controller Design

The control scheme is the following:

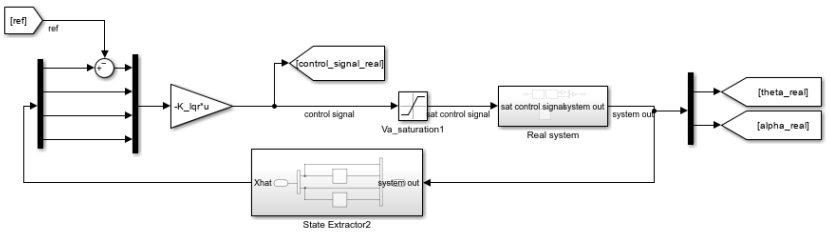

In order to design the LQ controller we choose the matrices Q and R to be diagonal and tweaked their values in order to weight more the state α, to make the tip aligned with the base as fast as possible, and the state θ to grant set point tracking.

$$Q = \begin{bmatrix} Q(1,1) & 0 & 0 & 0 \\ 0 & 1 & 0 & 0 \\ 0 & 0 & Q(3,3) & 0 \\ 0 & 0 & 0 & 1 \end{bmatrix} \text{ and } R = 1$$

We tried different values for Q and R and compared the main characteristics of a step response. A summary can be seen in the table below:

Q(1,1)	Q(3,3)	Max overshoot (°)	Settling time (s)	Rising time (s)	Total input (Vs)
1000	100	14.06	0.427	0.096	3.021
100	1000	-0.967	1.024	0.238	3.433
200	1000	1.494	0.853	0.174	2.411
100	2000	-0.615	1.280	0.274	2.957
1000	1000	9.316	0.466	0.108	3.383

4.4.2 Observers comparison

4.4.3 Validation

Step Response

Frequency Validation

Position Control of the Tip with Uncertanties

Conclusioni